WILEY | Hindawi

Research Article

A Visualized Method of Airflow between Adjacent Zones inside a Multizone Building Based on Pressure Difference Frequency: Airflow Mapping

Jiajun Jing,[1] Dong-Seok Lee,[2] Jaewan Joe,[3] Eui-Jong Kim,[3] Young-Hum Cho,[4] and Jae-Hun Jo [3]

[1]*Department of Architectural Engineering, Inha University, Incheon 22212, Republic of Korea*
[2]*Department of Architectural Engineering, Keimyung University, Daegu 42601, Republic of Korea*
[3]*Division of Architecture, Inha University, Incheon 22212, Republic of Korea*
[4]*School of Architecture, Yeungnam University, Gyeongsan 38541, Republic of Korea*

Correspondence should be addressed to Jae-Hun Jo; jhjo@inha.ac.kr

The airflow movement inside a multizone building has a significant impact on pollutant transfer, thermal comfort, and indoor air quality. However, there are difficulties in visualizing the airflow movement with existing methods. This study proposes a visualization method for evaluating airflows between adjacent internal zones inside a multizone building based on the analysis of pressure difference frequency. After the distribution of absolute pressure is measured and the wind pressures on the surfaces of the building are calculated, the variation of pressure differences between each couple of adjacent zones is analyzed for three levels: greater than 0 Pa, equal to 0 Pa, and less than 0 Pa (for any given zones selected as target zones). Finally, an airflow mapping is created for each floor using the visNetwork tool based on the R language. A target building was selected for applying the proposed method. The airflow mappings were derived from a detailed analysis of the pressure difference frequency between each couple of adjacent zones, presenting the variations of airflow direction and the dominant airflow during the measurement period in a visualized form. For example, the airflow direction from 1F_Z2 to 1F_Z3 is 92.0%. The spatial similarity in the variations of the airflow directions can also be observed on certain floors. The results of this experimental study show that the airflows between multiple zones can be easily identified without a complex building zone analysis. The variation in internal airflow direction between adjacent zones can be intuitively visualized, providing insight to the airtightness levels of building components. It is also observed that the airflow rates computed based on the airflow mappings can provide more guidance for the control of HVAC systems.

1. Introduction

Many buildings employ building management systems (BMS) combined with abundant sensors and sub-meters to monitor the variation of building environmental parameters and optimize the operational characteristics of their HVAC systems [1, 2]. However, most existing BMS cannot provide meaningful visual analytics that convert the measured data into visualized results to allow efficient interactions for building operators [3]. The existing visualization tools used in BMS are mainly for the visualization of energy use during HVAC system operation, where examples of such existing tools include Sankey diagrams [4], energy flow maps [5], and basic line or bar charts for analyzing and visualizing energy flows [6, 7].

However, building energy performance is highly related to airflow movement inside buildings, and airflow movement has a huge impact not only on energy consumption [8] but also on pollutant transfer [9] and occupants' thermal comfort [10], since the airflows inevitably transfer heat and gas or dust pollutants. In particular, the outbreak of the COVID-19 epidemic has drawn attention to the effect of

airflow patterns on the transmission of airborne diseases across indoor spaces [11]. Thus, it is necessary to analyze airflow movement for the operation of the HVAC system and for the control of indoor environmental parameters. In addition, if the visualization of the airflow movement can be integrated with the BMS, then building operators will be able to more readily understand and more efficiently optimize the control of building systems by interacting with the visualized results.

Airflow movement inside a multizone building is induced by a combination of driving forces created by the stack effect, wind effect, and mechanical systems [12]. The pressure differences across partitions drive airflow into, out of, and within a building when there are leakage paths in the partitions [13, 14]. Moreover, the complex airflows between internal zones are also influenced by various factors such as the zone layout, occupant behavior, and operation state of the HVAC system. Compared to indoor environmental parameters like temperature and humidity, it is a more challenging task to measure the variation of air movement between zones. In particular, the sizes of openings and the real-time variation of air velocity need to be measured before airflow rates can be calculated based on Bernoulli's equation. In some studies, thermal anemometers [15] or velocity profiling [16] have been applied for measuring air velocity at window openings. These techniques invariably lead to incorrect velocity magnitudes, especially for points with unsteady flow characteristics. Thus, there are technical difficulties in analyzing the airflow movement inside multizone buildings.

Experimental measurement and model simulation are two main methods available for evaluating airflow performance inside a multizone building. Field measurements are usually performed by either the multiple tracer gas technique [17] or the constant-concentration technique [18], which provide reliable quantitative information and address the air change rates between internal zones and between indoor and outdoor spaces. Some innovative methods such as the cyclic atmospheric CO_2 variation method [19] and the TMBE Kalman filtering method [20] allow the measurement of a fluctuating airflow rate. However, the field measurements above are mainly for evaluating the effect of ventilation inside buildings rather than for visualizing the airflow movement. For airflow visualization, particle image velocimetry (PIV) is usually used, which allows the visualization of complex internal flow patterns by tracking tracer particles seeded in the air to obtain the velocity field [21]. However, PIV is more suitable for small-scale measurements than full-scale measurements due to the fact that PIV is often restricted to a space having an unobstructed field of vision [21].

In order to assess the airflow patterns considering the dependencies on building geometry, opening configurations, and climatic conditions, modeling methods are frequently applied in evaluating the characteristics of airflows inside buildings [22]. Analytical and empirical models are used to evaluate the airflow rate using fluid flow equations. However, these models suffer from a large number of assumptions, simplifications, and approximations for closing the system of equations, which compromise the accuracy of the results [23]. Multizone network models are implemented to solve airflows between adjacent zones or between indoor and outdoor spaces [24]. These models represent the characteristics of zones using connected nodes that have homogeneous state parameters for temperature, contaminant concentration, and the like [25, 26]. Some researchers [27, 28] have performed detailed reviews of multizone network models. Several commercial programs based on multizone network models are available for use, such as CONTAM [29] and COMIS [30]. Johnson et al. [31] evaluated the natural ventilation performance of a building with four commonly used models. The results of the study by Johnson et al. show that the performance is closely related to certain coefficients such as the opening discharge coefficient and that the network models might be less accurate for large openings.

All in all, in the above methods for the analysis of airflow movement inside multizone buildings, there are difficulties in measuring the airflow rates by field measurements, and even if the airflow movements can be visualized by the PIV method, it is not suitable for the airflow analysis of an entire multizone building, as they cannot provide visualized airflow movement between each couple of adjacent zones in real time. As described before, airflows across building components are driven by pressure differences, and airflow rates are governed by the magnitude of the pressure differences and the airtightness level of the target components. In particular, the direction of airflows may change in accordance with the direction of the pressure differences [14]. In addition, airflow rates inside a building cannot be measured conveniently, whereas the pressure distribution in all zones of the building can be monitored in real time. Therefore, it is possible to monitor the magnitudes and directions of the pressure differences across building components from the pressure sensor network deployed inside a building. The pressure distribution of all zones can be derived from the monitored pressure values, and further, the visualization of airflow movement can be achieved by using a visualization tool. Especially for buildings with detailed requirements on airflow patterns, such as hospital operating rooms and negative pressure isolation wards (NPIW) [32], the airflow movement can be visualized just by monitoring the pressure distribution in each zone, allowing building operators to easily apply their knowledge and take actions against the variation of airflows.

In this study, a visualization method for airflow movement is developed by analyzing the pressure difference frequency between each couple of adjacent zones. The method can convert the measured pressure values into useful visual representations and present the airflow mapping of each floor. The visualization method is also demonstrated by actual pressure data collected from a 4-story multizone building located in South Korea, and the airflow mapping of each floor is finally presented. The visualization method can also be integrated with the BMS to provide more comprehensive information for building operators.

2. Methodology

2.1. Driving Forces for Airflow Movement inside a Multizone Building. The airflows between adjacent zones are driven by

pressure differences induced by a combination of the stack effect (ΔP_s), wind effect (ΔP_w) and mechanical systems (ΔP_m), as shown in [33]

$$\Delta P_t = \Delta P_s + \Delta P_w + \Delta P_m. \tag{1}$$

ΔP_s is mainly derived from the compound impact of a temperature difference and a height difference between indoor and outdoor air, which create airflows across the building's envelope and interior components [33], and is usually the dominant force driving airflow movement in a high-rise building, especially during cold periods [34]. It can also be seen that a greater temperature difference and a greater building height usually lead to larger stack pressure differences.

ΔP_w highly depends on wind speeds, wind angles acting on building surfaces, the building shape, and conditions of the surrounding area [17]. Furthermore, wind speeds and wind pressures on a building façade all increase significantly with building height, resulting in a wide pressure range over the building façade [35]. Upper floors experience larger wind pressures than lower floors. Also, during mild weather conditions, ΔP_w is usually very low for low-rise buildings. The relative importance of ΔP_s and ΔP_w in a building is closely related to the building height, internal resistance, and building envelope [17].

ΔP_m is determined by the directions of supply and return air volumes and the difference in these flows, leading to the various patterns of indoor air balance [17]. The regulation of indoor static pressure should make sure that all airflows entering through openings in the building envelope are balanced by the airflows induced by mechanical equipment. In particular, the zones in which the supply air volume is greater usually have a higher absolute air pressure compared with other zones [36].

2.2. Outline of the Suggested Visualization Method for Airflow Movement. It is widely acknowledged that the direction of airflow across any building component is mainly maintained by the direction of the pressure difference and that the related airflow rates are determined by the magnitude of the pressure difference and the airtightness level of the target component. Moreover, corridor pressurization or differential pressure instrumentation is also employed inside buildings to regulate the airflow movement based on the changing pressure difference. As mentioned before, it is possible to obtain the pressure variation of all zones with pressure sensors equipped in each zone and evaluate the airflow movement from an analysis of the directions and magnitudes of the pressure differences. Therefore, this study proposes a method for evaluating the airflow movement between each couple of adjacent zones based on a frequency analysis of the pressure difference and visualizing the evaluated results. The suggested method can provide detailed information on the spatial relations between internal zones and can present visualized results of the changing airflow directions between adjacent zones. As shown in Figure 1, this method consists of 5 steps: (I) establishing a database for pressure distribution; (II) obtaining the variation of pres-

sure difference (ΔP); (III) analyzing the variation of ΔP frequency between adjacent zones; (IV) evaluating the airflow movement between adjacent zones; and (V) visualizing the airflow movement between adjacent zones. The detailed procedures for each step are as shown below:

Step I: Establishing a database for pressure distribution.

  (i) A pressure sensor device is installed in each zone of each floor, and the variation of absolute pressure with time is monitored

  (ii) The variation of wind pressure on each side of the building façade is also calculated by using the local wind conditions provided by a weather station

Step II: Obtaining the variation of the pressure difference (ΔP).

  (i) The spatial relationships between zones are identified by field investigations

  (ii) Based on the spatial connections, the real-time pressure difference (ΔP) of each couple of adjacent zones and the wind pressure difference acting on each zone are calculated

Step III: Analyzing the variation ΔP frequency between adjacent zones.

  (i) Based on the variation of ΔP, the ΔP frequencies are analyzed at three levels for each target zone according to the magnitude of the ΔP

Level 1: frequency of ΔP being less than 0
Level 2: frequency of ΔP being equal to 0
Level 3: frequency of ΔP being larger than 0

  (ii) The ΔP frequency analysis is performed for all zones, and the frequency results are summarized for each floor

Step IV: Evaluating the airflow movement between adjacent zones.

  (i) A target zone is first selected, and all zones adjacent to this zone are identified. For example, the adjacent zones of target zone Z1 are Z2, Z3, and Z4

  (ii) The pressure difference frequency results for the corresponding adjacent zones are identified. For example, the frequency variation of the pressure difference between Z1 and Z2 (two adjacent zones) is identified

  (iii) The airflow movement between selected adjacent zones is evaluated based on the pressure frequency results. For example, when the ΔP between Z1 and Z2 is greater than 0 with a frequency of 70%, this indicates that the airflow direction is from Z1 to Z2 at 70% frequency. In contrast, the airflows move from Z2 to Z1 at frequency of 10% when the ΔP is smaller than 0
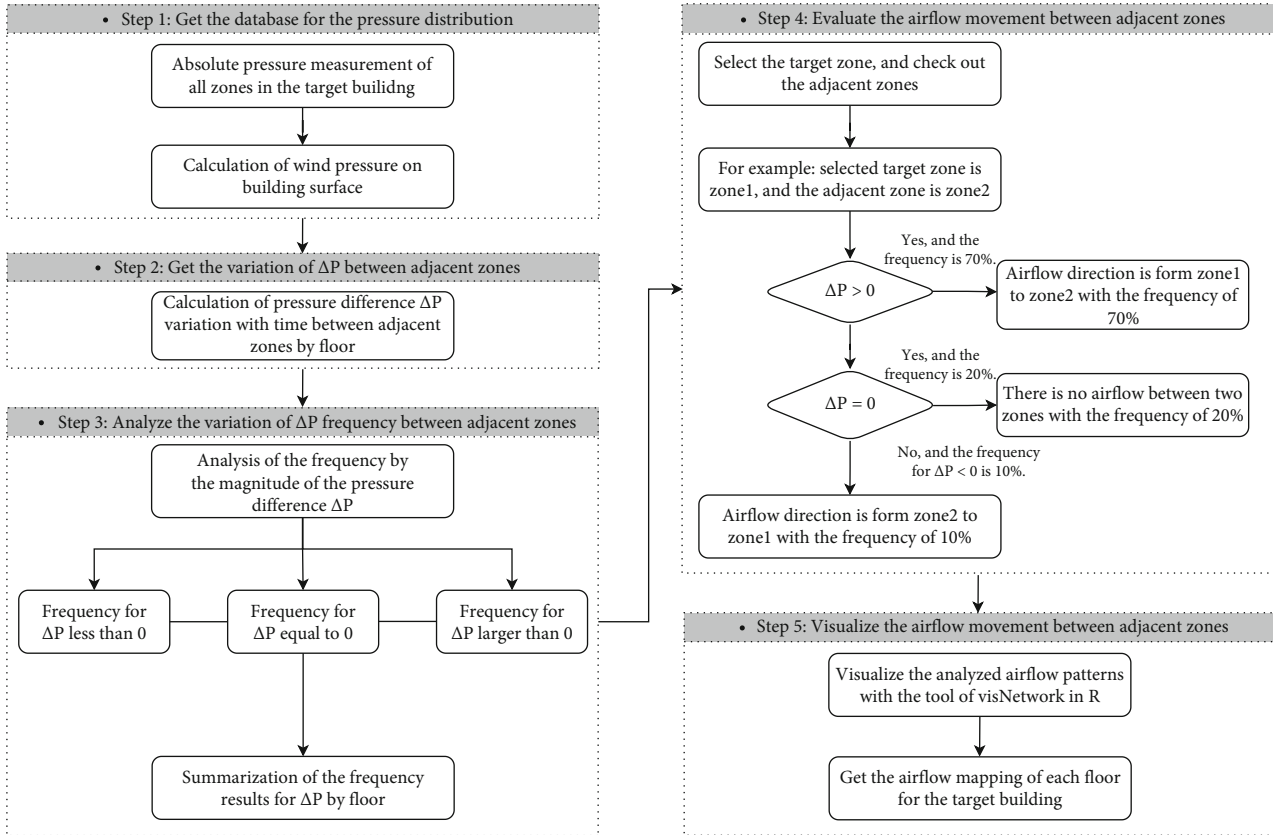
FIGURE 1: Flowchart of the proposed method.

(iv) The analyzed results are obtained for all adjacent zones on each floor

Step V: Visualizing the airflow movement between adjacent zones

(i) The evaluated results for the airflow direction variation between each couple of adjacent zones are organized into a table by floor

(ii) The airflow movement is visualized with the R package tool visNetwork [37]

(iii) The airflow mapping of each floor is obtained

As in the detailed explanation of the method provided above, the airflow mappings of each floor can be finally derived, and the variation of the airflow direction between each couple of adjacent zones can also be identified by the intuitive visualization of airflow movement.

3. Pressure Data Collection in a Multizone Low-Rise Building

For verifying the applicability of this proposed method, 24-hour pressure measurements were performed inside a real multizone building. The following sections present a description of the target building and instrumentation used, as well as a detailed explanation of the absolute pressure and wind pressure values collected in the real building.

3.1. Building Description. The measured building is a 4-story multizone office building located in Incheon, Republic of Korea. The specifications of the building are shown in Figure 2. In the floor plan of the building, each story is connected by the atrium, and staircases run between the downstairs and upstairs. Two elevators and one staircase are installed in this building for vertical traffic. A curtain wall system serves as the envelope for this target building. There is no central HVAC system installed in the building, with split air conditioners and the multi split systems of air conditioners employed instead in some rooms for heating and cooling. Also, there are no exhaust fans or other ventilators in either the restrooms or other rooms. The total number of interior zones is 22, as shown in Figure 2(b), with 4 zones for the 1st floor, 5 zones for the 2nd floor, 4 zones for the 3rd floor, and 9 zones for the 4th floor, separately.

3.2. Absolute Pressure Measurement of Internal Zones. Due to the fact that the airflow between adjacent zones is driven by the pressure difference, the field measurement was taken on a windy day, and the windows and doors between measured zones were closed for developing an apparent understanding of the pressure difference between adjacent zones. A 24-hour field measurement of all zones in this target

(a) Outside view

(b) Zone distribution in the floor plan

FIGURE 2: Specifications of the target building.

TABLE 1: Instrument specifications.

Instrument	Picture	Specifications
Pressure monitoring system A (data receiver and logger)		Communication: RF communication Function: receive real-time measured data from multiple B systems
Pressure monitoring system B (pressure sensors)		Model: model PTB110 Range: 800 to 1100 hPa Accuracy: ±0.30 hPa at +20°C Repeatability: ±0.03 hPa Interval: 5 s (minimum) Storage: 8 GB Function: monitor real-time absolute pressure and communicate with system A
Absolute pressure gauge (standard absolute pressure)		Model: model PTB330 class A Range: 500 to 1100 hPa Accuracy: ±0.10 hPa at +20°C Repeatability: ±0.03 hPa Function: monitor real-time absolute pressure and provide standard value

building was carried out in this study. Unlike temperature and humidity, the absolute pressure on the floor surface always remains the same everywhere in a single zone, and a large pressure difference cannot be detected between different points on the floor surface. Therefore, the absolute pressure in each zone shown in Figure 2 was measured at the floor surface of the zones simultaneously by using the self-developed absolute pressure monitoring systems A and B shown in Table 1. For this measurement, 2 system A and 22 system B were deployed inside the target building. The limited number of system B was connected to a system A by a wireless network. System A serves as a data receiver and processor, and system B serves for absolute pressure monitoring. The system B with a repeatability of ±0.03 hPa allows accurate determination of the pressure fields even if the accuracy falls to ±0.30 hPa compared with external ambient air pressure. Also, the absolute pressure value detected by the absolute pressure gauge acts as a reference air pressure rather than the exterior ambient air pressure. All of the devices were calibrated to the reference pressure values before the actual measurement. Thus, the pressure difference relationships between adjacent zones were able to be accurately determined under an allowable repeatability of ±0.03 hPa.
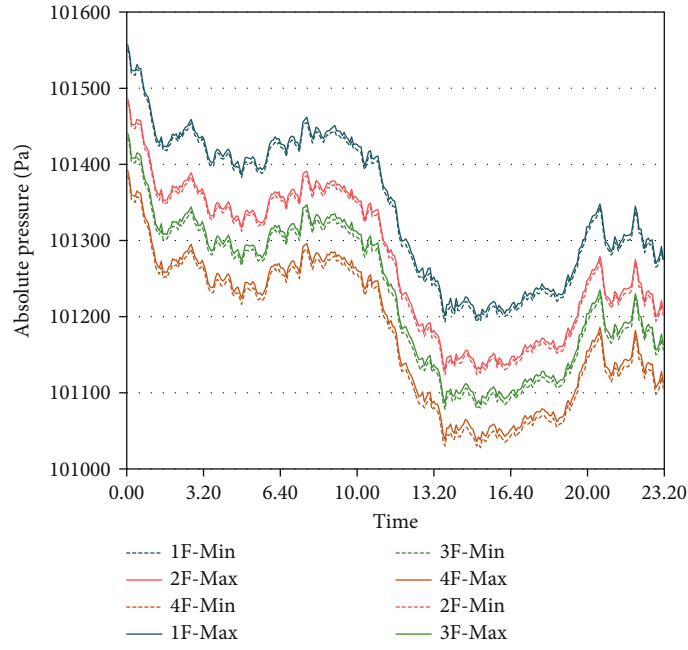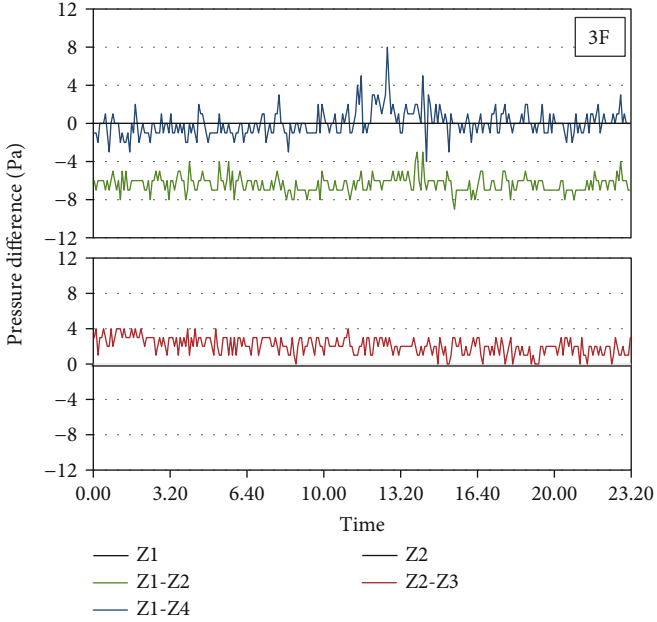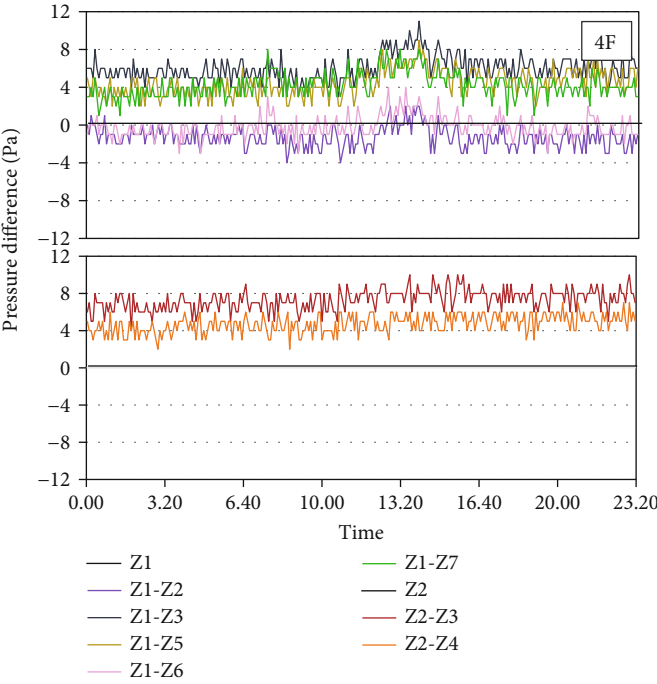
(a)
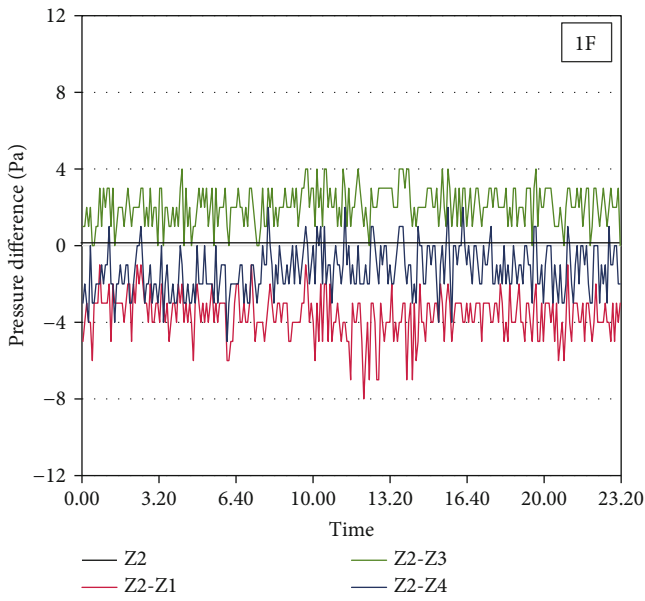
(b)
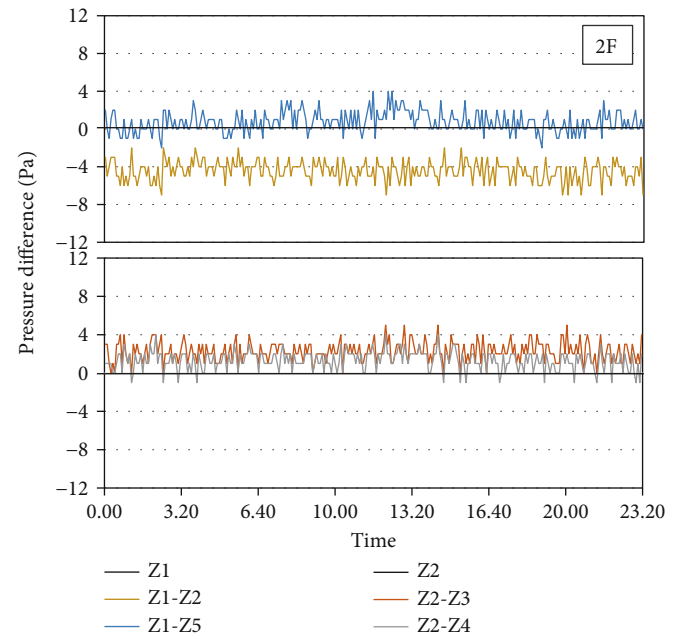
(c)

Figure 3: Continued.
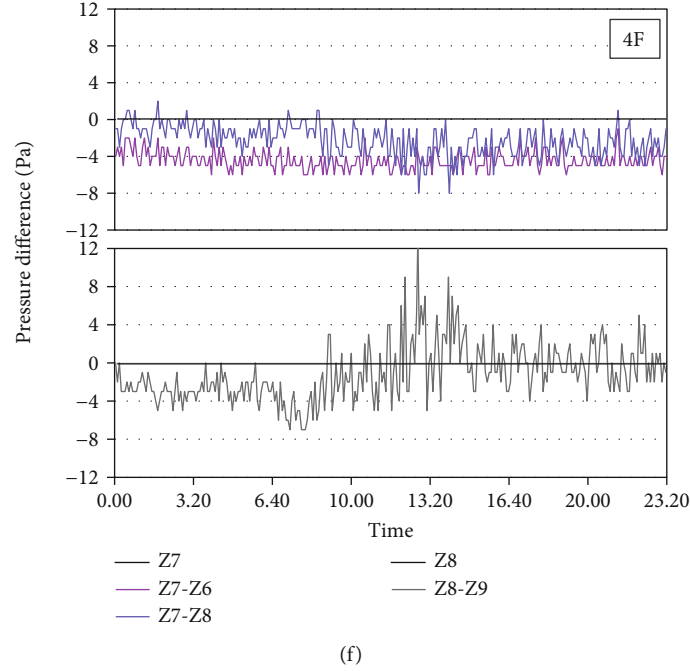
(d)

(e)

FIGURE 3: Continued.

FIGURE 3: Pressure distribution in the target building: (a) Variation of absolute pressure with time on each floor. (b–f) Pressure difference between adjacent zones on each floor.

TABLE 2: Recommended values for the atmospheric boundary layer parameters.

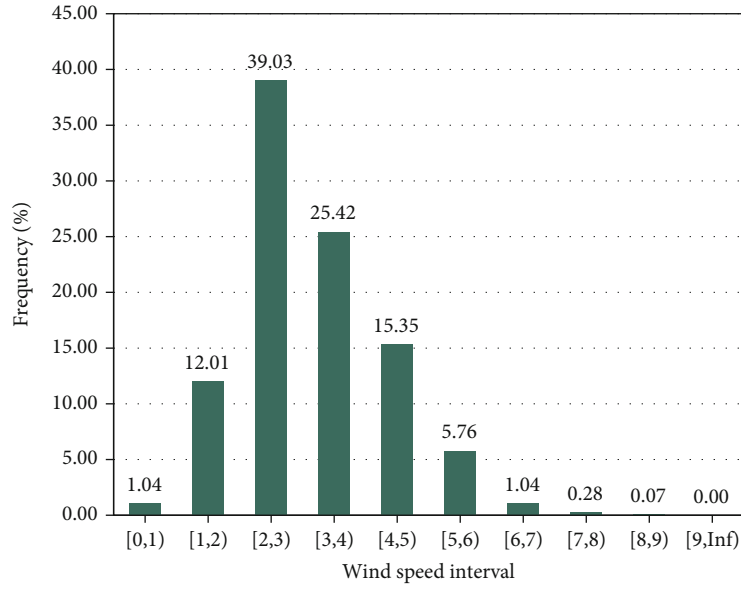| Description	Exponent a	Layer thickness δ (m)
Large city centers	0.33	460
Urban and suburban areas, wooded areas, etc.	0.22	370
Open terrain with scattered obstructions having heights less than 9 m	0.14	270
Flat, unobstructed areas	0.10	210

The measured overall pressure distribution in all of the zones in the target building is shown in Figure 3. Although the overall tendencies of absolute pressure over time on different floors are similar among zones, as shown in Figure 3(a), there are still effective pressure differences between adjacent zones which can significantly impact the airflow movement between zones on the same floors as shown in Figures 3(b)–3(d). Therefore, the collected data on the pressure difference between adjacent zones is suitable for verifying this proposed method.

3.3. Estimation of Wind Pressure on Building Surface. As mentioned before, wind also causes variable surface pressure on the building envelope that has an apparent effect on air infiltration and exfiltration and is thus especially relevant when considering changes in interior pressures. Generally, wind creates a positive pressure on the windward face and a negative on the roof and leeward face of a building, causing outside air to flow from the windward faces toward the leeward faces [17]. The wind pressure can be calculated as Equation (2) [17]. In particular, the approach wind speed U_H in Equation (3) is always estimated by the wind speed U_{met} from the local meteorological station, with corrections applied in regard to terrain and height, as shown in [17]

$$P_w = C_P \rho_a \frac{U_H^2}{2},\tag{2}$$

$$U_H = U_{met} \left(\frac{\delta_{met}}{H_{met}}\right)^{a_{met}} \left(\frac{H}{\delta}\right)^a.\tag{3}$$

Here, P_w is the wind surface pressure relative to outdoor static pressure in undisturbed flow (Pa); C_P is the dimensionless wind pressure coefficient; ρ_a is outdoor air density in kg/m^3; U_H is the approach wind speed at the height of the upwind wall; U_{met} is the hourly wind speed from a meteorological station in m/s; δ_{met} is the atmospheric boundary layer thickness for the meteorological station in m (typical value: 270 m); δ is the wind boundary layer thickness for the local building terrain in m; H_{met} is the height of the meteorological station in m (typical value: 10 m); H is the wall height in m; a_{met} is the dimensionless atmospheric boundary exponent for the meteorological station (typical value: 0.14); and a is the atmospheric boundary layer exponent for the local building terrain. ASHARE 2017 [17] provides the detailed values for the atmospheric boundary layer parameters a and δ, as shown in Table 2, and exponent

(a) Wind speed Frequency (%)

Wind rose

Wind speed in m/s

☐ V⩾9   ☐ 8⩽V<9
☐ 7⩽V<8   ☐ 6⩽V<7
☐ 5⩽V<6   ☐ 4⩽V<5
☐ 3⩽V<4   ☐ 2⩽V<3
☐ 1⩽V<2   ☐ 8⩽V<1
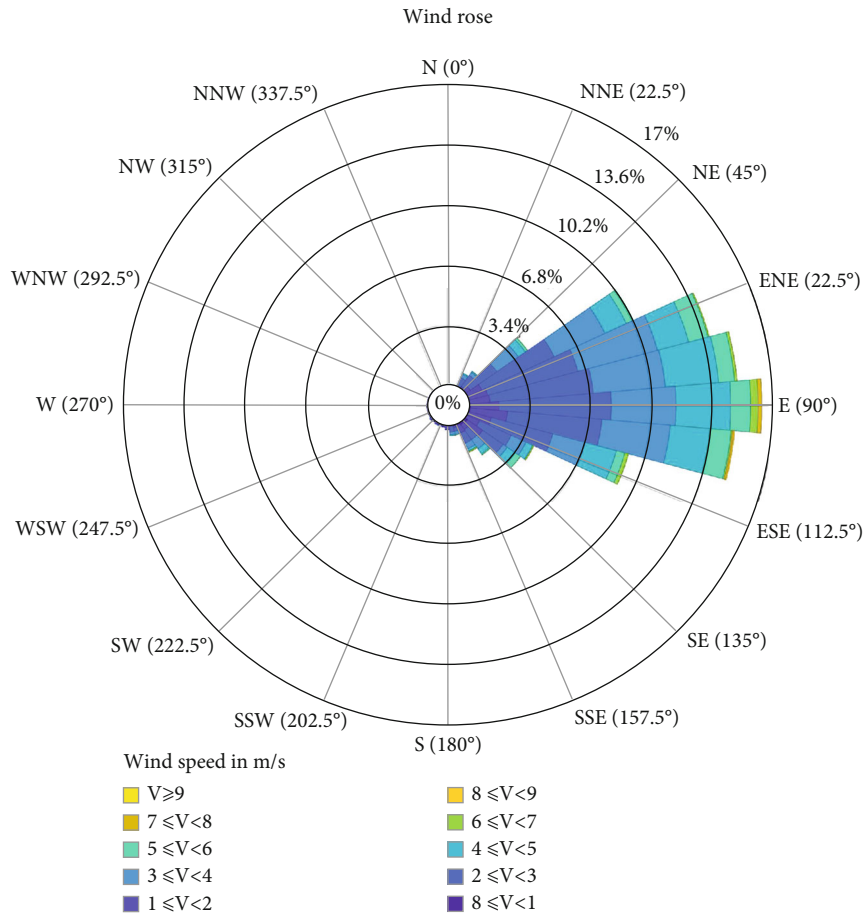
(b) Wind direction distribution

Figure 4: Wind conditions of Incheon on Sept. 3rd.

a for 0.22 and layer thickness δ for 370 m are suitable for this target building based on the actual location of this building.

The wind conditions during the measurement period are shown in Figure 4, and there were no extreme conditions such as high-speed wind lasting for an extended time. The frequency of the wind speed in the [2,3) interval was the highest with 39.03%, and the mean wind speed was 3.13 m/s. It is reasonable to consider the major wind direction of 89°
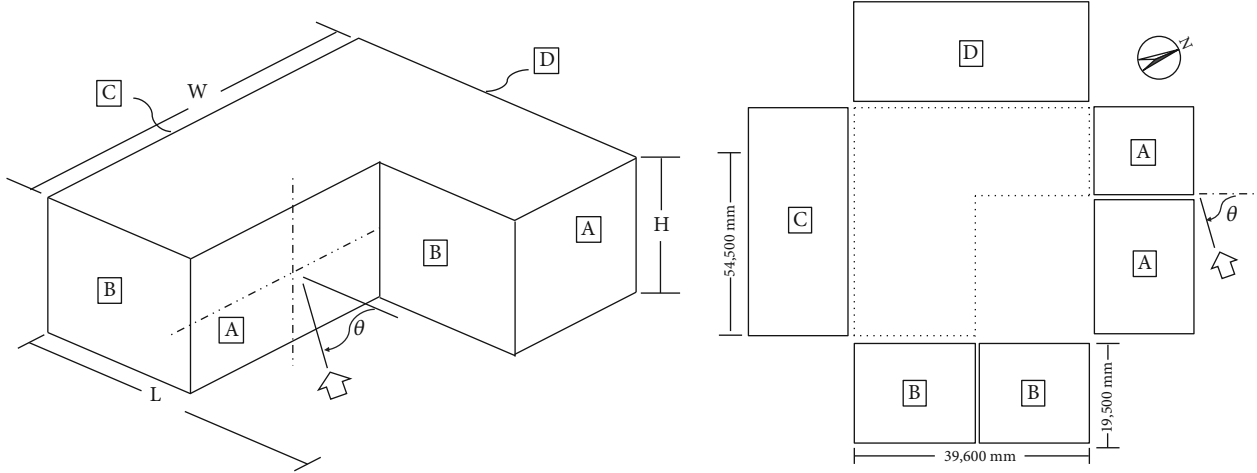
FIGURE 5: Building geometry with building sides a–d; dimensions L, W, and H; wind angle θ.

(almost the E direction) to represent the wind direction during the measurement period due to the fact that the wind direction changed in a narrow range shown in Figure 4(b).

As shown in Equation (2), the wind pressure coefficient C_P is the most important factor affecting the surface wind pressure of the envelope. However, costly wind tunnel model tests or full-scale tests are required for a completely accurate determination of C_P, especially when used for a high-rise building [38]. For a low-rise building, parametric equations are mainly applied to estimate the value, and the method provided by Swami and Chandra is frequently adapted by researchers [39, 40], as shown in Equation (4). Swami and Chandra also suggested that $C_P(0\circ)$ value of 0.6 can be probably used for all low-rise buildings.

$$
\begin{aligned}
C_P = C_P(0\circ) \ln \Big[& 1.248 - 0.703 \sin \frac{\theta}{2} - 1.175 \sin^2\theta \\
& + 0.131 \sin^3(2G\theta) + 0.769 \cos \frac{\theta}{2} \\
& + 0.07G^2 \sin^2 \frac{\theta}{2} + 0.717 \cos^2 \frac{\theta}{2} \Big].
\end{aligned}
\tag{4}
$$

Here, C_P is the dimensionless wind pressure coefficient; θ is the wind angle measured from the normal direction of a building surface; and G is the natural log of side ratio length to width.

Due to the fact that the wind direction changed almost around the major direction of 89°, as shown in Figure 4(b). The related wind angle for each side of this target building also did not change a lot correspondingly. Figure 5 shows the geometry of the building with sides a–d. The wind angles θ of each side were determined based on the major wind direction of 89°. The wind angles were measured from the normal of each side to the wind direction, and the results for the sides a–d were 51°, 39°, 129°, and 141°, respectively. Especially, according to Equation (4), the magnitude and sign of C_P on each side will not change significantly due to a relatively stable wind angle and the low value for $C_P(0\circ)$. Therefore, the C_P value during measurement time for each

TABLE 3: Wind pressure coefficient of each side for target building.

Building sides	Wind angle	Aspect ratio (W/L)	Wind pressure coefficient (C_P)
A	51°	1.38	0.26
B	39°	1.38	0.39
C	129°	1.38	-0.41
D	141°	1.38	-0.31

building side can be regarded as fixed in this study. Table 3 shows the C_P value obtained for each side, as calculated in accordance with Equation (4). It is observed that the A and sides were windward faces with positive values of 0.26 and 0.39, while the C and D sides were leeward faces with negative values of -0.41 and -0.31.

The wind pressure on the building surfaces of each floor was estimated using (Equations (2)–(4)). Figure 6 shows the wind pressure distribution during the measurement period on each side of each floor. It can be seen that building surface pressures increased with building height. The A and B sides were under positive pressure, and the C and D sides were under negative pressure during the measurement period. Even though there were occasional occurrences of huge wind pressure acting on the building surfaces, the total distributions of wind pressure varied lightly and always remained within a narrow range from the distribution obtained for low wind pressure. For example, the wind pressures for the A side for the 4th floor of the 25th–75th percentiles were within the range of 0.57–1.51 Pa due to the influence of the low wind speeds. Even though the magnitude of wind pressure was not large enough to produce significant influence for the variation of indoor pressure during the measurement period, the sign of the wind pressure on each side always remains fixed due to the relatively stable wind direction, which means that the estimated wind pressure with clear direction is suitable for verifying this proposed method.
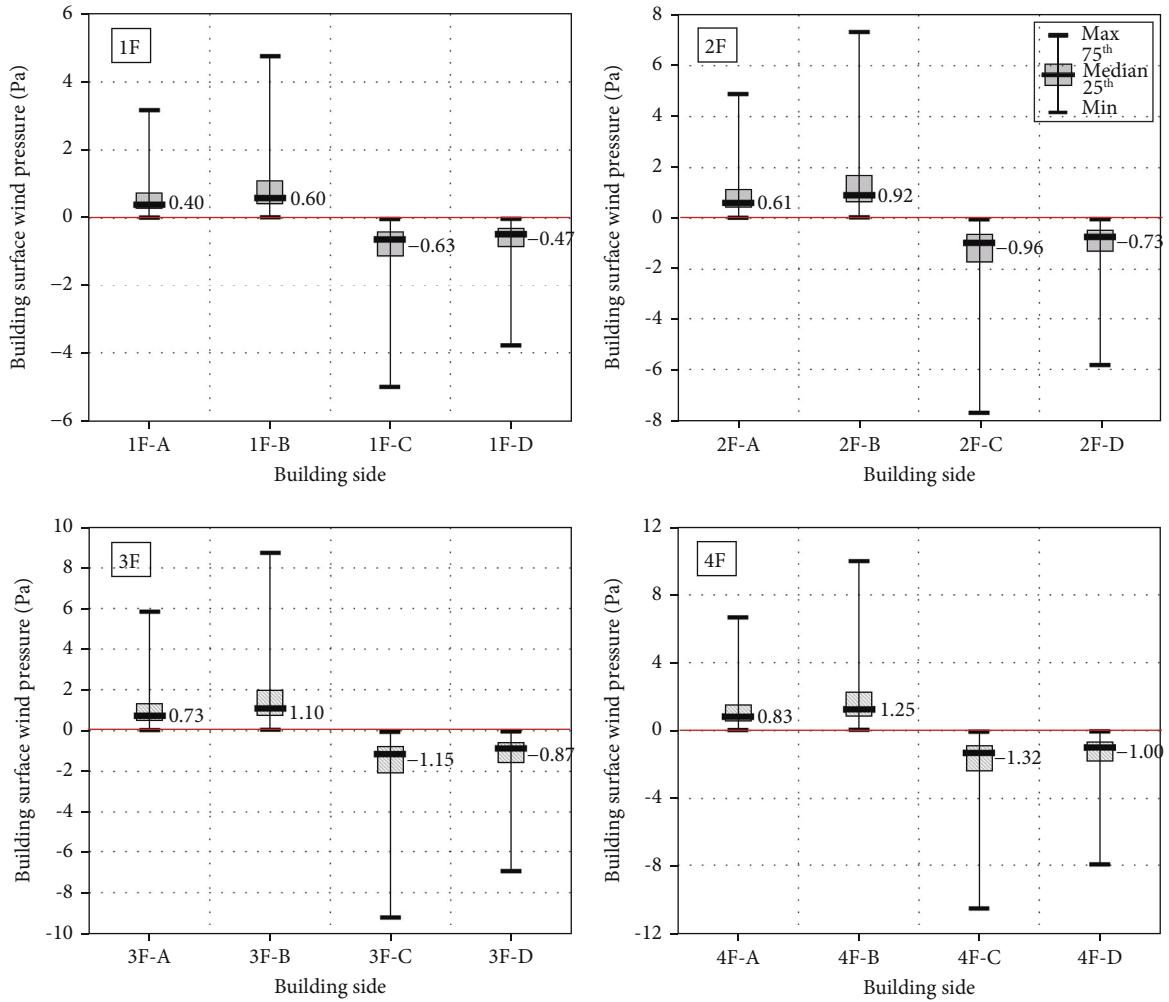
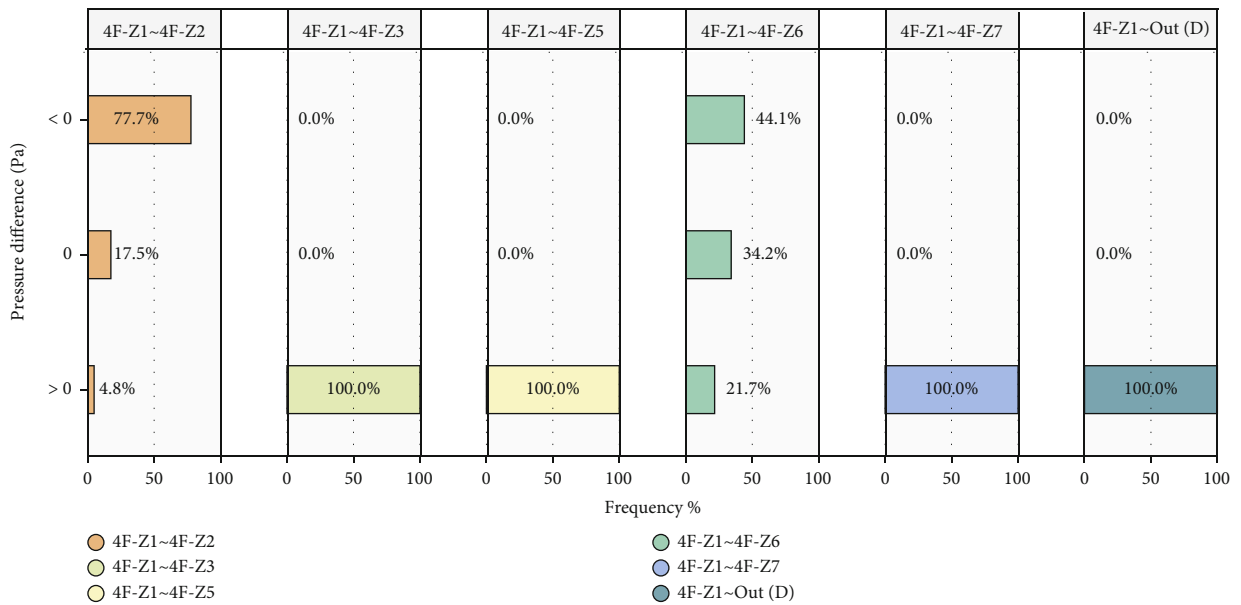FIGURE 6: Wind pressure distribution on the exterior surfaces of the building on each floor.

FIGURE 7: Example of analysis for ΔP level frequency for each adjacent zone of Z1 on the 4th floor.

Table 4: Example of ΔP level frequency between adjacent zones for all zones on the 4th floor.

ΔP	4F-Z1 (%)			4F-Z2 (%)			4F-Z3 (%)			4F-Z4 (%)			4F-Z5 (%)		
	>0	=0	<0	>0	=0	<0	>0	=0	<0	>0	=0	<0	>0	=0	<0
Z1	—	—	—	77.7	17.5	4.8	0	0	100	—	—	—	0	0	100
Z2	4.8	17.5	77.7	—	—	—	0	0	100	0	0	100	—	—	—
Z3	100	0	0	100	0	0	—	—	—	—	—	—	—	—	—
Z4	—	—	—	100	0	0	—	—	—	—	—	—	—	—	—
Z5	100	0	0	—	—	—	—	—	—	—	—	—	—	—	—
Z6	21.7	34.2	44.1	—	—	—	—	—	—	—	—	—	—	—	—
Z7	100	0	0	—	—	—	—	—	—	—	—	—	—	—	—
Z8	—	—	—	—	—	—	—	—	—	—	—	—	—	—	—
Z9	—	—	—	—	—	—	—	—	—	—	—	—	—	—	—
Out	100	0	0	0	0	100	—	—	—	0	0	100	100	0	0

ΔP	4F-Z6 (%)			4F-Z7 (%)			4F-Z8 (%)			4F-Z9 (%)			Out (%)		
	>0	=0	<0	>0	=0	<0	>0	=0	<0	>0	=0	<0	>0	=0	<0
Z1	44.1	34.2	31.7	0	0	100	—	—	—	—	—	—	0	0	100
Z2	—	—	—	—	—	—	—	—	—	—	—	—	100	0	0
Z3	—	—	—	—	—	—	—	—	—	—	—	—	—	—	—
Z4	—	—	—	—	—	—	—	—	—	—	—	—	100	0	0
Z5	—	—	—	—	—	—	—	—	—	—	—	—	0	0	100
Z6	—	—	—	0	0	100	—	—	—	—	—	—	0	0	100
Z7	100	0	0	—	—	—	86.7	10.7	2.6	—	—	—	0	0	100
Z8	—	—	—	2.6	10.7	86.7	—	—	—	63.5	11.8	24.7	100	0	100
Z9	—	—	—	—	—	—	24.7	11.8	63.5	—	—	—	100	0	100
Out	100	0	0	100	0	0	100	0	100	100	0	100	—	—	—

—: not adjacent zone.

4. Airflow Mapping of the Target Multizone Low-Rise Building

4.1. Frequency Distribution of Pressure Difference between Adjacent Zones. As shown in Figure 1 of Section 2.2, after the measurement of absolute pressure in each zone and the calculation of wind pressures on the building surfaces in step I, the pressure difference (ΔP) between each couple of adjacent zones of each floor should be calculated in accordance with step II. The wind pressure on each side was regarded as the ΔP between the inside of each zone and the outside. The ΔP values are divided into three levels (>0, =0, and <0) by magnitude. Then, the frequency distributions of ΔP were analyzed to determine the variation of airflow directions through certain building partitions, as shown in step III.

Figure 7 shows an example of Z1 on the 4th floor for the frequency analysis of ΔP. There are 6 adjacent zones in Z1: Z2, Z3, Z5, Z6, Z7, and the D side of the building. The figure shows a significant frequency variation of ΔP for the three levels between each couple of adjacent zones. For Z3, Z5, Z7, and out (D), the frequency of ΔP being greater than 0 was 100%. For Z2 and Z6, the frequency of ΔP being less than 0 was the highest, with values of 77.7% and 44.1%, respectively. Apparently, the frequency of ΔP for Z1~out (D) is 100% due to the fixed direction of wind pressure on the D side of this target building. Then, the frequencies of the ΔP levels between adjacent zones of all floors were

analyzed by this process. Table 4 shows an example of the ΔP frequency results on the 4th floor, where the variations of ΔP frequency between all adjacent zones on the 4th floor are listed.

4.2. Airflow Mapping of each Floor. After analyzing the frequency distribution of the ΔP levels between adjacent zones according to step III, shown in Figure 1, the airflow movement should be evaluated based on step IV. The frequency results of the 4th floor are used as an example below to explain the process of step IV in Figure 1 regarding evaluating the variation of airflow directions between relevant adjacent zones.

As shown in Table 4, among all the adjacent zones of the 4th floor, i.e., the pairs of Z1 and Z2, Z1 and Z6, Z7 and Z8, and Z8 and Z9, the relative magnitudes of ΔP between the zones varied for three levels of greater than 0, equal to 0, and less than 0 with various frequency distributions, indicating that the airflow directions also changed accordingly. For example, taking Z1 as the target zone, the ΔP frequencies between Z1 and Z2 for the levels of greater than 0, equal to 0, and less than 0 are 4.8%, 17.5%, and 77.7%, respectively, indicating that the frequency of airflow from Z1 to Z2 is 4.8%, the frequency of no airflow between the two zones is 17.5%, and the frequency of airflow from Z2 to Z1 is 77.7%. Although the airflow direction between Z1 and Z2 was not constant, the airflow during the measurement

period mainly flowed from Z2 to Z1 according to the highest frequency of the three levels. The ΔP values between the remaining adjacent zones all remained within a single level of either the greater than 0 level or the smaller than 0 level with a corresponding frequency of 100%, showing that the airflow movements between these adjacent zones remained constant during the measurement period. For Z8 and Z9, the ΔP values relative to the building exterior changed between the two levels of the greater than 0 level and the less than 0 level with a frequency of 100%, indicating that there is more than one side adjacent to the building exterior. This is because the major wind direction for the measurement period is fixed as the average direction of 89°, and the sign of the wind pressure coefficient for each side of the building is also unchanged. The airflow direction is further determined by the magnitudes of ΔP for the related sides, and the airflow direction is constant on each side with a frequency of 100%.

Although the airflow movement between adjacent zones can be evaluated according to step IV, it is impossible to obtain intuitive results for the variation of the airflow directions based on ΔP frequency analysis. As such, it is necessary to visualize the evaluated results in step IV if the airflow movement is to be controlled directly in a more detailed manner. In this study, the visNetwork tool is employed to visualize the evaluated results derived by step IV. The visNetwork tool is an R package for displaying the interactive visualization of networks such as social networks, citation networks, trade networks, and others [37]. This study innovatively applies the tool to the field of building indoor airflow analysis, to visualize the relationships among adjacent internal zones and the frequencies of airflow direction changes between adjacent zones. The visualized results of airflow movement are referred to here as the airflow mapping of the target floor.

Figure 8 shows the airflow mapping of all floors for depicting the layout of the zones, adjacent relationships among zones, and changing airflow directions with frequencies generated by step IV. Figure 8(a-1) presents the main idea using visNetwork to visualize the airflow movement based on pressure difference frequency. In Figure 8(a-1), green nodes refer to the internal zones of the 1st floor of the target building, and red nodes represent the outside of the building for the A~D sides. Brown edges correspond to adjacent relationships connecting inside zones, while the arrows refer to the airflow directions with their respective frequencies. Blue edges connecting green and red nodes display the airflow movements between internal zones and the outside of the building. Then, the related frequency for airflow movement is combined with the information of adjacent relationships, deriving the airflow mapping for the 1st floor by the visNetwork tool shown in Figure 8(a-2). Figures 8(b)–8(d) show the airflow mappings for other floors.

The airflow mappings make it possible to identify the adjacent relationships between zones without having to refer to the complex building floor plan. For instance, the adjacent zones of Z2 on the 1st floor are Z1, Z3, Z4, and the A side, C side, and D side of the building. The adjacent zones of Z1 on the 2nd floor are Z5 and Z2 and the D side of the building.

Moreover, based on the adjacent relationships, the variation of airflow directions can be directly expressed by the arrows, and the significant differences in the changing frequencies can also be indicated. For example, on the 1st floor, the direction of airflow was always from Z1 to Z2 with a 100% frequency. The airflow direction between Z4 and Z2 was not constant during the measurement period, and the airflow from Z4 to Z2 was with a frequency of 75.7%, while the frequency for the airflow from Z2 to Z4 is 7.6%. In particular, there was no airflow passing between the two zones with a frequency of 16.7%. Moreover, although the airflow direction between many adjacent zones changed significantly, the dominant airflow direction during the measurement period could be determined from the magnitudes of ΔP frequency. For example, on the 1st floor, the airflow direction was mainly from Z2 to Z3 with a corresponding frequency of 92.0%, and on the 4th floor, the airflow between Z1 and Z2 mainly flowed from Z2 to Z1 with a 77.7% frequency.

Interestingly, spatial similarity in the variations of internal airflow movement was readily observable between different floors in the airflow mappings, which occurred due to the underlying similar spatial distribution of the zones on these floors. For instance, the areas and locations of Z1, Z2, and Z5 on the 2nd floor are approximately consistent with Z1, Z2, and Z4 on the 3rd floor. According to the airflow mappings of the two floors, the variation of airflow directions between these zones was similar during the measurement period. For Z1 and Z2 on the 2nd floor, and Z1 and Z2 on the 3rd floor, the airflow directions between the adjacent zones were fixed during the measurement period with a constant direction from Z2 to Z1, and the corresponding frequencies were 100%. In addition, for Z1 and Z5 on the 2nd floor and Z1 and Z4 on the 3rd floor, there were changing airflow directions, with almost identical frequencies of absent airflow between the adjacent zones at 33.0% and 32.3%, respectively.

All in all, with the help of the airflow mapping by floor, the complex variation of internal airflow between zones can be visualized intuitively without the cumbersome measurement work of airflow rates or the model simulation for the analysis of a building's internal airflow movement.

5. Discussion and Limitations

5.1. Airflow Rates between Adjacent Internal Zones. In this study, cracks around doors between each couple of adjacent zones are considered to be the main airflow paths of each floor because doors typically present significantly greater leakage areas than internal walls. Due to the lack of airtightness data for components in this measured building, this study refers to the effective leakage area (ELA) for doors at the reference pressure difference of 4 Pa recommended by ASHRAE 2001 to represent the airtightness parameters of doors existing between adjacent zones [41]. Although the recommended values would not be identical to the actual airtightness, the differences in airtightness levels between various types of doors would correspond to the actual
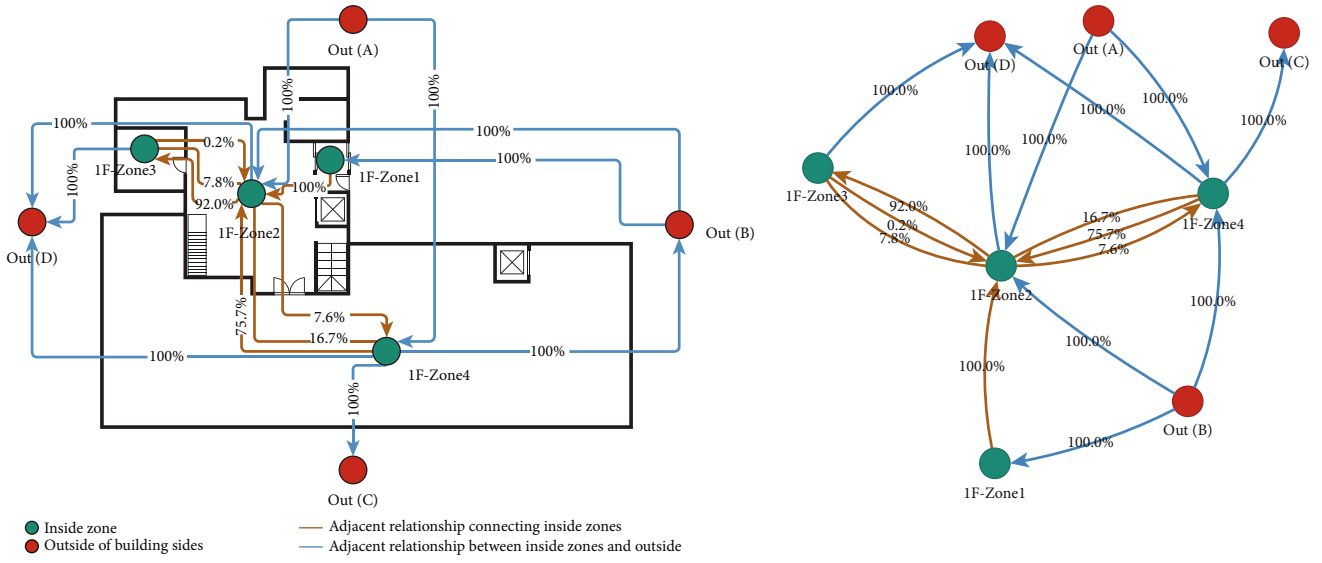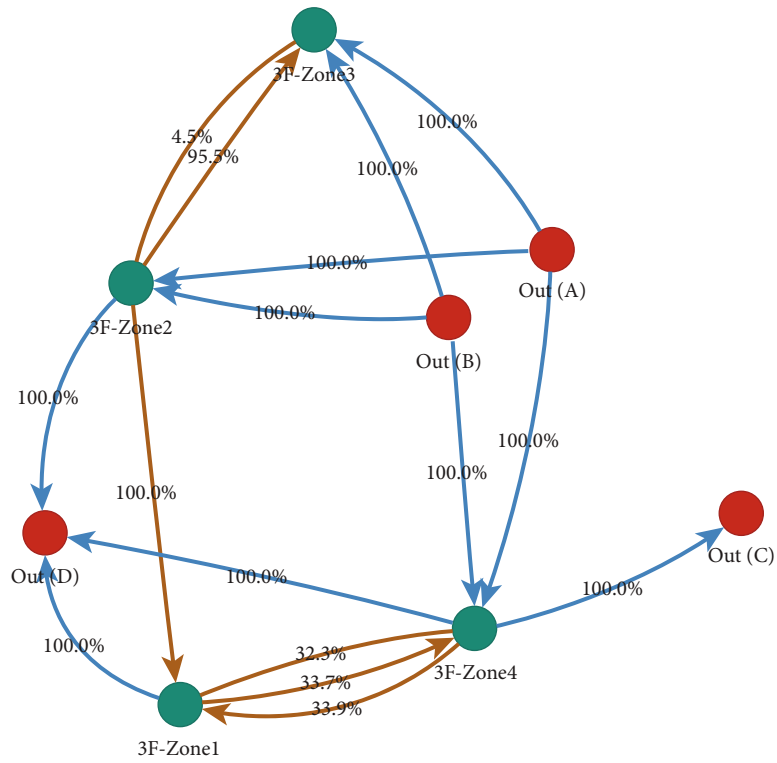
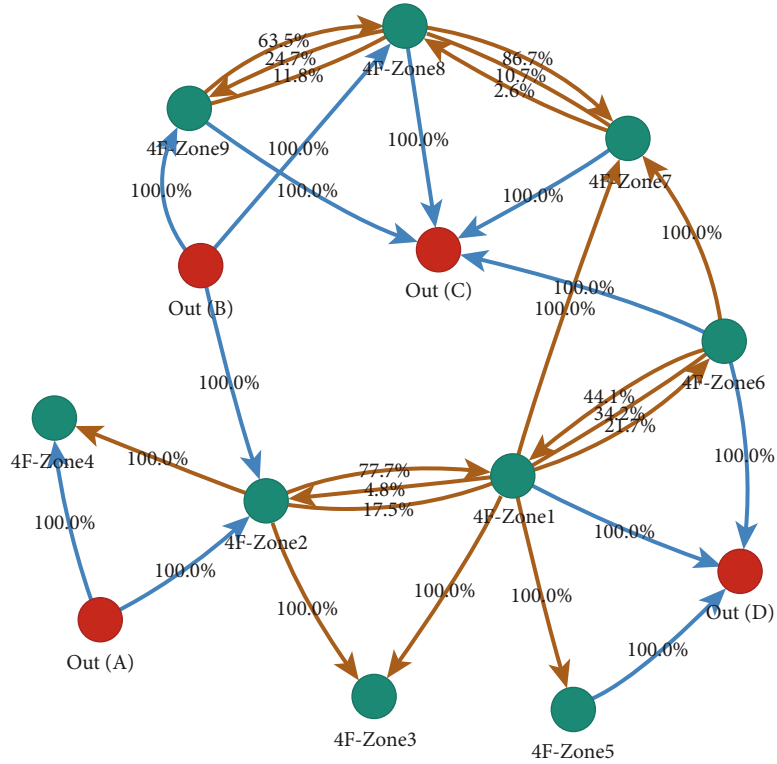(a) (a-1, a-2) Airflow mapping of the 1st floor
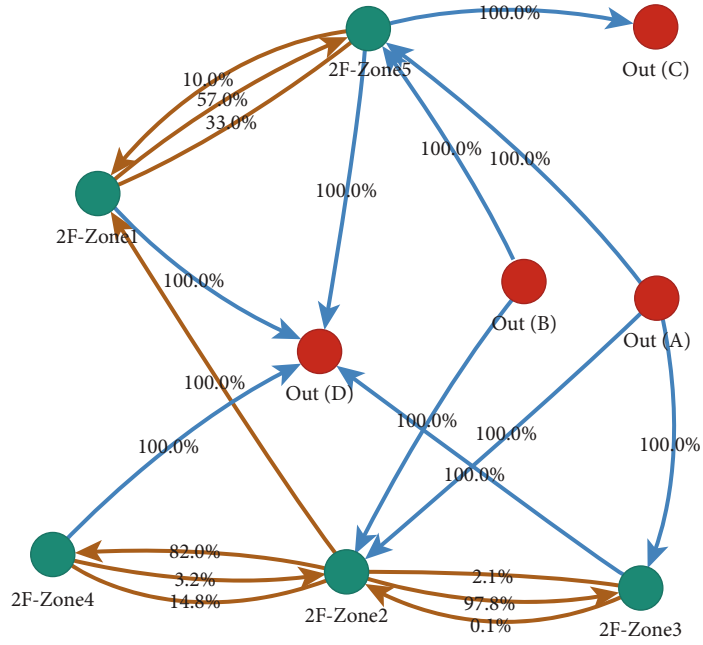
(b) Airflow mapping of the 2nd floor

FIGURE 8: Continued.

(c) Airflow mapping of the 3rd floor

(d) Airflow mapping of the 4th floor

FIGURE 8: Airflow mapping of each floor.

TABLE 5: Types of doors between adjacent zones of 4th floor.

Adjacent zones	Type of door	Effective leakage area (cm^2)
Z1- Z2	Sliding, double, glass	22
Z1- Z3	Swinging, single, weather-stripped	12
Z1- Z5	Swinging, single, glass, not weather-stripped	21
Z1- Z6	Swinging, interior, double, metal	14
Z1- Z7	Swinging, interior, double, metal	14
Z2- Z3	Swinging, single, glass, not weather-stripped	21
Z2- Z4	Swinging, single, glass, not weather-stripped	21
Z6- Z7	Swinging, interior, double, metal	14
Z7- Z8	Swinging, interior, double, metal	14
Z8- Z9	Swinging, interior, double, metal	14

situation. Table 5 shows the types of doors included on the 4th floor.

Based on the airflow mappings and the air leakage data of building components, it was found that the variation of airflow movement between adjacent zones is closely related to the types of doors or, more specifically, to the relative magnitudes of airtightness levels. As shown in Table 5, the same types of doors with high airtightness levels are used between Z1 and Z6, Z7 and Z8, and Z8 and Z9. These doors are closed most of the time, and the directions of airflow through these doors always changed for the three levels as presented on the airflow mapping of the 4th floor. Even though the types of doors between Z1 and Z7 and between Z6 and Z7 are also the same as the doors mentioned above, the airflow directions are constant because the airtightness levels of the two doors decrease gradually with frequent use of these two doors. Conversely, the types of doors between Z2 and Z3, Z2 and Z4, and Z1 and Z5 are the same as each other with a lower airtightness level, and the airflow directions were constant during the measurement period. Therefore, the airflow directions always change for doors having high-level airtightness, and the airflow directions are always constant for doors having low-level airtightness.

The airflow directions maintained by pressure differences are easily evaluated by the airflow mappings of each floor, and the variation of airflow rates between adjacent zones can be analyzed according to the distribution of pressure differences and air leakage data. Moreover, the detailed airflow rates between adjacent zones are especially important if the HVAC system is to be used to balance the airflows of the supply system and exhaust system. The airflow rate under any certain pressure difference can be expressed by the following equation [41], where it is determined from the leakage area at a reference pressure difference value.

$$Q_{r,2} = \frac{C_{D,1}A_{r,1}}{10000}\sqrt{\frac{2}{\rho}}(\Delta P_{r,1})^{0.5-n}(\Delta P_{r,2})^n. \quad (5)$$

Here, $Q_{r,2}$ is the airflow rate in the measured pressure difference $\Delta P_{r,2}$ (m^3/s); $C_{D,1}$ is the discharge coefficient; $A_{r,1}$ is the air leakage area at the reference pressure difference $\Delta P_{r,1}$ (cm^2); and $\Delta P_{r,1}$ is the reference pressure (Pa). The discharge coefficient and reference pressure difference are always applied to two situations: $\Delta P_{r,1}$ equals 4 Pa and $C_{D,1}$ equals 1 or $\Delta P_{r,1}$ equals 10 Pa and $C_{D,1}$ equals 0.611 [41]. n is the flow exponent, which usually lies between 0.6 and 0.7 [41]. In this study, a value of 1 for $C_{D,1}$ at 4 Pa and a coefficient of 0.65 for n are utilized.

Figure 9 shows the average airflow rates between all couples of adjacent zones on the 4th floor during the measurement period, where the related frequency results derived from the airflow mapping are also marked in the figure. The figure shows significant differences in airflow rates between the adjacent zones having different frequencies. The airflow rates from Z1 to Z5, Z2 to Z3, and Z2 to Z4 all exceeded 20 m^3/h with a corresponding frequency of 100%. The airflow rates from Z2 to Z1, Z1 to Z3, Z1 to Z7, and Z6 to Z7 were all between 10 m^3/h and 15 m^3/h, and the corresponding frequency from Z2 to Z1 was 77.7% and 100% for the others. For the adjacent zones Z1 and Z6, Z7 and Z8, and Z8 and Z9 in particular, although the airflow directions between these zones were uncertain during the measurement period, the airflow rates were all less than 10 m^3/h. As such, guidance for regulating the distribution of airflow rates and controlling the pressure difference of HVAC systems can be provided based on a detailed analysis of the airflow rates between all adjacent zones. For example, the pressure differences or airflow rates between Z1 and Z5, Z2 and Z3, and Z2 and Z4 should be adjusted preferentially due to their high airflow rates and fixed airflow directions. In contrast, for Z1 and Z6, Z7 and Z8, and Z8 and Z9, there is no need for regulating the pressure differences or the airflow rates between these zones since there are changes in airflow direction but the airflow rates are low.

5.2. Strengths and Limitations of This Study. This study demonstrates that the airflow movement between any adjacent zones can be visualized intuitively with the measurement of absolute pressure. The airflow mapping of each floor, derived with the tool visNetwork, makes it possible to meticulously control airflow movement without having to consider the layout of the target floor. This study also suggests that the airtightness levels of doors between adjacent zones have an apparent impact on the variation of airflow movement between these zones, indicating that the airflow
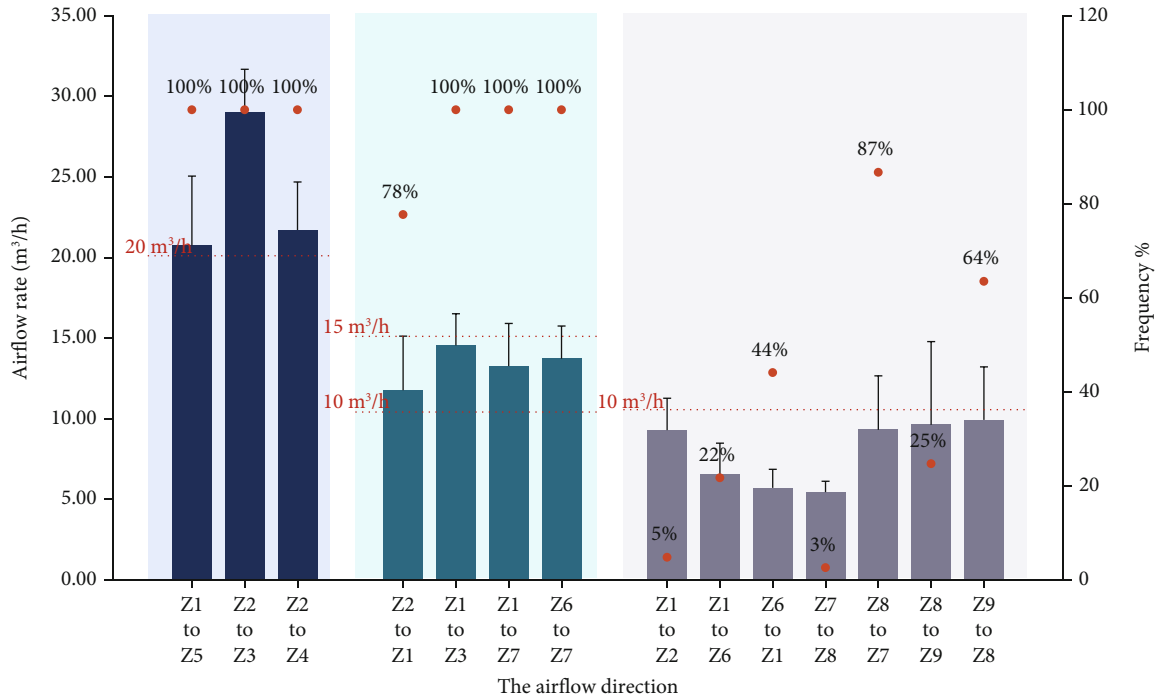
FIGURE 9: Average airflow rates between adjacent zones on 4th floor.

direction across the doors with high airtightness level always change with low airflow rates.

Some limitations of this study should also be addressed. The field pressure measurements were only conducted for 24 hours. Moreover, the outdoor wind speed was not high, resulting in low wind pressures on the surfaces of the building and hence no significant effect on the fluctuations of indoor pressure. The real-time variability of local wind on a building enclosure is not considered in this study, and only one boundary condition of the major wind direction is applied for the determination of wind pressure coefficients. The classification of wind conditions needs to be considered for a more accurate representation of the local wind effects on the building enclosure. Long-term monitoring of absolute pressure values in all zones can aid the researcher in accumulating daily or monthly airflow mappings during various weather conditions to summarize the general airflow movement between adjacent zones. Also, it should be noted that there are only 22 zones in the measured building, and the number of zones on the 1st floor~3rd floor in particular is limited. The layout and number of zones also have an impact on the airflow movement between adjacent zones. For future studies, field measurements can be taken on a more complex building to verify the proposed method and confirm our conclusions. It is also necessary to perform the airtightness measurements for specific building components so as to evaluate the actual airflow rates between adjacent zones using the derived airflow mappings. In addition, due to the lack of a central air conditioning system and other ventilation devices in the measured building, it was not possible to regulate the airflows or pressures based on the results. The applicability and effectiveness of using HVAC systems to regulate airflow rates between adjacent zones

should be explored along with the derived conclusions, in a future study.

6. Conclusion

The airflow movement inside a building has a significant impact on the indoor air quality and the energy consumption of the building system. However, there are many obstacles to visualizing the complex airflow movement between adjacent zones and between the interior and exterior spaces of a building with existing methods. The objective of this study is to propose a convenient method for visualizing airflow movement inside a multizone building. To this end, the absolute pressure measurements in each zone of each floor should be performed first, and the airflow movement is then visualized in accordance with a ΔP frequency analysis through the tool visNetwork provided in the R language. Field pressure measurements were conducted in a 4-story multizone building, and the airflow mappings were obtained from a detailed analysis of the ΔP frequency for all adjacent zones on each floor. The results show that the variation of internal airflow direction can be visualized intuitively between adjacent zones and that the dominant airflow during the measurement period can also be determined from the relative magnitudes of the frequencies. For example, the airflow movement was mainly from Z2 to Z3 on the 1st floor with a frequency of 92.0%. The spatial similarity in the variations of airflow directions was also indicated between the 2nd and 3rd floors, and the airflow movement between Z2 and Z1 were the same with a constant airflow direction of 100% frequency. The calculated results of airflow rates can also provide guidance for the regulation of HVAC systems. If the airflow mappings can be integrated

with the BMS for a target building in the future, building operators and researchers would be able to control airflow conditions quickly and make accurate responses for a smarter operation the building system.

For future studies, it would be desirable to conduct long-term measurements in more complex multizone buildings, considering the impact of various local weather conditions and multiquantity zones on internal airflow movement. Also, the pressure control and airflow regulation of HVAC systems between adjacent zones need to be identified based on the visualized airflow mappings, considering the exact airtightness levels of building components.

Data Availability

Data are available from the corresponding authors upon request of the readers.

Disclosure

We would like to mention that the contents of this study have been preprinted before and are available at SSRN: https://ssrn.com/abstract=4334321 or doi:10.2139/ssrn.4334321.

Conflicts of Interest

The authors declare that they have no known competing financial interests or personal relationships that could have appeared to influence the work reported in this paper.

Authors' Contributions

Jiajun Jing performed the methodology, measurement, data curation, writing the original draft, investigation, and visualization. Dong-Seok Lee did the preparation and visualization. Jaewan Joe, Eui-Jong Kim, and Young-Hum Cho were assigned in writing which includes review and discussion. Jae-Hun Jo did the conceptualization, writing which includes review and discussion, and supervision.

Acknowledgments

References

[1] A. Abdelalim, W. O'Brien, and Z. Shi, "Data visualization and analysis of energy flow on a multi-zone building scale," *Automation in Construction*, vol. 84, pp. 258–273, 2017.

[2] L. K. Murugesan, R. Hoda, and Z. Salcic, "Visualization of electricity consumption: software prototype through literature survey," *International Journal of Innovative Research in Science, Engineering and Technology*, vol. 3, pp. 2725–2729, 2014.

[3] D. Darwazeh, B. Gunay, J. Duquette, and W. O'Brien, "A virtual meter-based visualization tool to present energy flows in multiple zone variable air volume air handling unit systems," *Building and Environment*, vol. 221, article 109275, 2022.

[4] A. Abdelalim, W. O'Brien, and Z. Shi, "Development of Sankey diagrams to visualize real HVAC performance," *Energy and Buildings*, vol. 149, pp. 282–297, 2017.

[5] D. B. Belzer, *Energy End-Use Flow Maps for the Buildings Sector*, Pacific Northwest National Lab.(PNNL), Richland, WA, USA, 2006.

[6] I. Yarbrough, Q. Sun, D. C. Reeves, K. Hackman, R. Bennett, and D. S. Henshel, "Visualizing building energy demand for building peak energy analysis," *Energy and Buildings*, vol. 91, pp. 10–15, 2015.

[7] H. Truong, A. Francisco, A. Khosrowpour, J. E. Taylor, and N. Mohammadi, "Method for visualizing energy use in building information models," *Energy Procedia*, vol. 142, pp. 2541–2546, 2017.

[8] C. Chen and B. Zhao, "Review of relationship between indoor and outdoor particles: I/O ratio, infiltration factor and penetration factor," *Atmospheric Environment*, vol. 45, no. 2, pp. 275–288, 2011.

[9] I. Stasiulaitiene, E. Krugly, T. Prasauskas et al., "Infiltration of outdoor combustion-generated pollutants to indoors due to various ventilation regimes: a case of a single-family energy efficient building," *Building and Environment*, vol. 157, pp. 235–241, 2019.

[10] M. Fan, Z. Fu, J. Wang et al., "A review of different ventilation modes on thermal comfort, air quality and virus spread control," *Building and Environment*, vol. 212, article 108831, 2022.

[11] A. Bhattacharya, J. Pantelic, A. Ghahramani, and E. S. Mousavi, "Three-dimensional analysis of the effect of human movement on indoor airflow patterns," *Indoor Air*, vol. 31, no. 2, pp. 587–601, 2021.

[12] F. A. Iaq, E. Health, and L. E. Buildings, "Air flow in high rise multi unit residential building with respect to ventilation and IAQ," in *ASHRAE IAQ 2013 Proceedings: Environmental health in low energy buildings*, pp. 477–481, Peachtree Corners, GA, USA, 2013.

[13] C. Younes, C. A. Shdid, and G. Bitsuamlak, "Air infiltration through building envelopes: a review," *Journal of Building Physics*, vol. 35, no. 3, pp. 267–302, 2012.

[14] C. H. Lozinsky and M. F. Touchie, "Inter-zonal airflow in multi-unit residential buildings: a review of the magnitude and interaction of driving forces, measurement techniques and magnitudes, and its impact on building performance," *Indoor Air*, vol. 30, no. 6, pp. 1083–1108, 2020.

[15] M. Caciolo, P. Stabat, and D. Marchio, "Full scale experimental study of single-sided ventilation: analysis of stack and wind effects," *Energy and Buildings*, vol. 43, no. 7, pp. 1765–1773, 2011.

[16] N. Nikolopoulos, A. Nikolopoulos, T. S. Larsen, and K. S. P. Nikas, "Experimental and numerical investigation of the tracer gas methodology in the case of a naturally cross-ventilated building," *Building and Environment*, vol. 56, pp. 379–388, 2012.

[17] ASHRAE, "2017 ASHRAE Handbook—Fundamentals," in *Chapter 16: Vent. Infiltration*, American Society of Heating, Refrigerating and Air-Conditioning Engineers, 2017.

[18] W. Pan, S. Liu, Y. Wang, X. Cheng, H. Zhang, and Z. Long, "Measurement of cross-ventilation rate in urban multi-zone dwellings," *Building and Environment*, vol. 158, pp. 51–59, 2019.

[19] J. Dias Carrilho, M. Mateus, S. Batterman, and M. Gameiro Da Silva, "Air exchange rates from atmospheric CO_2 daily cycle," *Energy and Buildings*, vol. 92, pp. 188–194, 2015.

[20] R. Duarte, M. Glória Gomes, and A. Moret Rodrigues, "Estimating ventilation rates in a window-aired room using Kalman filtering and considering uncertain measurements of occupancy and CO_2 concentration," *Building and Environment*, vol. 143, pp. 691–700, 2018.

[21] X. Cao, J. Liu, N. Jiang, and Q. Chen, "Particle image velocimetry measurement of indoor airflow field: a review of the technologies and applications," *Energy and Buildings*, vol. 69, pp. 367–380, 2014.

[22] G. Remion, B. Moujalled, and M. El Mankibi, "Review of tracer gas-based methods for the characterization of natural ventilation performance: comparative analysis of their accuracy," *Building and Environment*, vol. 160, article 106180, 2019.

[23] S. Omrani, V. Garcia-Hansen, B. Capra, and R. Drogemuller, "Natural ventilation in multi-storey buildings: design process and review of evaluation tools," *Building and Environment*, vol. 116, pp. 182–194, 2017.

[24] Q. Chen, "Ventilation performance prediction for buildings: a method overview and recent applications," *Building and Environment*, vol. 44, no. 4, pp. 848–858, 2009.

[25] L. Wang, W. S. Dols, and Q. Chen, "Using CFD capabilities of CONTAM 3.0 for simulating airflow and contaminant transport in and around buildings," *HVAC&R Research*, vol. 16, no. 6, pp. 749–763, 2010.

[26] L. Wang and Q. Chen, "Evaluation of some assumptions used in multizone airflow network models," *Building and Environment*, vol. 43, no. 10, pp. 1671–1677, 2008.

[27] A. C. Megri and F. Haghighat, "Zonal modeling for simulating indoor environment of buildings: review, recent developments, and applications," *HVAC&R Research*, vol. 13, no. 6, pp. 887–905, 2007.

[28] J. Axley, "Multizone airflow modeling in buildings: history and theory," *HVAC&R Research*, vol. 13, no. 6, pp. 907–928, 2007.

[29] W. S. Dols and B. Polidoro, *CONTAM User Guide and Program Documentation: Version 3.2*, US Department of Commerce, National Institute of Standards and Technology, 2015.

[30] B. V. Feustel and H. E. Smith, *COMIS 3.0–User's Guide*, Lawrence Berkeley National Laboratory, Berkeley, CA, USA, 1997.

[31] M. H. Johnson, Z. J. Zhai, and M. Krarti, "Performance evaluation of network airflow models for natural ventilation," *HVAC&R Research*, vol. 18, pp. 349–365, 2012.

[32] J. Guo, J. Liu, D. Tu, J. Zhang, J. Xu, and P. Xue, "Multizone modeling of pressure difference control analyses for an infectious disease hospital," *Building and Environment*, vol. 206, article 108341, 2021.

[33] D. S. Lee, K. H. Ji, J. Jing, and J. H. Jo, "Experimental study on elevator door reopening problems caused by stack induced pressure differences across the elevator door in buildings," *Building and Environment*, vol. 221, article 109271, 2022.

[34] J. H. Jo, J. H. Lim, S. Y. Song, M. S. Yeo, and K. W. Kim, "Characteristics of pressure distribution and solution to the problems caused by stack effect in high-rise residential buildings," *Building and Environment*, vol. 42, no. 1, pp. 263–277, 2007.

[35] M. H. Günel and H. E. Ilgin, *Tall Buildings: Structural Systems and Aerodynamic Form*, Routledge, 2014.

[36] T. Lim, J. Cho, and B. S. Kim, "Predictions and measurements of the stack effect on indoor airborne virus transmission in a high-rise hospital building," *Building and Environment*, vol. 46, no. 12, pp. 2413–2424, 2011.

[37] T. Almende, B. V. Thieurmel, and B. Robert, "visNetwork: Network visualization using vis.jslibrary," 2019, https://cran.r-project.org/package=visNetwork.

[38] R. T. Muehleisen and S. Patrizi, "A new parametric equation for the wind pressure coefficient for low-rise buildings," *Energy and Buildings*, vol. 57, pp. 245–249, 2013.

[39] M. Swami and S. Chandra, "Procedures for calculating natural ventilation airflow rates in Buildings, ASHRAE Final Rep. FSEC-CR-163-86," 1987, http://scholar.google.com/scholar?hl=en&btnG=Search&q=intitle:Procedures+for+Calculating+Natural+Ventilation+Airflow+Rates+in+Buildings#0%5Cnhttp://scholar.google.com/scholar?hl=en&btnG=Search&q=intitle:Procedures+for+calculating+natural+ventilation+airfl.

[40] M. V. Swami and S. Chandra, "Correlations for pressure distribution on buildings and calculation of natural-ventilation airflow," *ASHRAE Transactions*, vol. 94, pp. 243–266, 1988.

[41] ASHRAE, *ASHRAE Handbook—Fundamentals, Chapter 26: Ventilation and Infiltration*, American Society of Heating, Refrigerating and Air-Conditioning Engineers, Atlanta, GA, USA, 2001.